Science of the Total Environment 797 (2021) 149025

Contents lists available at ScienceDirect

Science of the Total Environment

journal homepage: www.elsevier.com/locate/scitotenv

Sulfur dynamics in forest soil profiles developed on granite under contrasting climate conditions

Zhuojun Zhang [a,d], Hairuo Mao [a], Zhi-Qi Zhao [b,*], Lifeng Cui [c], Shilu Wang [a], Cong-Qiang Liu [c,*]

[a] State Key Laboratory of Environmental Geochemistry, Institute of Geochemistry, Chinese Academy of Sciences, Guiyang 550081, China
[b] School of Earth Science and Resources, Chang'an University, Xi'an 710054, China
[c] Institute of Surface-Earth System Sciences, Tianjin University, Tianjin 300072, China
[d] University of Chinese Academy of Sciences, Beijing 100049, China

HIGHLIGHTS

- S in soils formed from granite is derived mainly from decomposing litter.
- Cold/dry climate results in S accumulation at the surface.
- Warm/wet climate results in S retention in the subsurface.
- Pedogenic Fe/Al minerals play a key role in retaining soil S.
- A conceptual model of S dynamics in soil profiles of different climate is proposed.

GRAPHICAL ABSTRACT

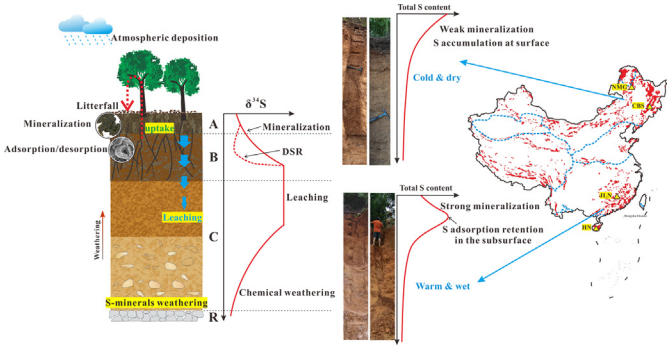

ARTICLE INFO

Article history:
Received 14 April 2021
Received in revised form 15 June 2021
Accepted 9 July 2021
Available online 15 July 2021

Editor: Manuel Esteban Lucas-Borja

Keywords:
Sulfur dynamics
Soil profiles
Granite
Climate
Stale sulfur isotope

ABSTRACT

Sulfur (S) dynamics in soils formed from granite remain poorly understood despite its importance as an essential plant macronutrient and component of soil organic matter. We used stable S isotope ratios to trace the sources and biogeochemical processes of S in four forest soil profiles developed on granite under contrasting climate conditions. The soil S is derived mainly from decomposing litter; no significant geogenic contribution to its content is noted as a result of the low S concentration of the granite (~ 5 μg/g). Colder/drier climate results in high organic S retention at the surface due to weak mineralization of organic S. Although warmer/wetter climate increases the S mineralization and leaching loss, SO_4^{2-} adsorption is an important S retention process in the subsurface. The vertical distribution of S isotope compositions in the soil profiles across the four sites indicates (i) a downward increase in $\delta^{34}S$ values in the upper profiles due to continuous mineralization of organic S with an occasional decrease in $\delta^{34}S$ values in the subsurface due to dissimilatory sulfate reduction (DSR), (ii) constantly high $\delta^{34}S$ values in the middle profiles due to the low water permeability, and (iii) a downward decrease in $\delta^{34}S$ values in the low profiles due to increased contribution of bedrock with depth. Regardless of the variation in soil depth and climate, the total S concentration is proportional to the pedogenic Fe/Al minerals, suggesting the important role of secondary Fe/Al minerals in retaining S in soils. This study provides an integration and synthesis of controls of climatic and edaphic variables on S dynamics in forest soil profiles developed on granite.

1. Introduction

Sulfur (S) is an essential macronutrient that forms quantitatively important components of structural and metabolic compounds in plants

* Corresponding authors.
E-mail addresses: zhaozhiqi@chd.edu.cn (Z.-Q. Zhao), liucongqiang@tju.edu.cn (C.-Q. Liu).

https://doi.org/10.1016/j.scitotenv.2021.149025
0048-9697/

and thus plays an important role in plant growth and development in response to various abiotic and biotic stresses (Freney and Williams, 1983; Marschner, 2011). In fact, a recently emerging problem of S deficiency has resulted in decreased crop yields and quality (Eriksen, 2009; Eriksen et al., 2004; Wilhelm Scherer, 2009). The main factors responsible for S dynamics include weathering of parent material, atmospheric deposition, mineralization of organic S, adsorption/desorption of SO_4^{2-}, dissimilatory sulfate reduction (DSR), and loss through leaching (Hermes et al., 2021; Mayer et al., 1995; Migaszewski et al., 2013; Novák et al., 2001; Schoenau and Bettany, 1989; Tanikawa et al., 2009; Zhang et al., 2014), all of which play different roles in various ecosystems. Moreover, S dynamics have been investigated in agricultural soil (e.g., Hermes et al., 2021; Solomon et al., 2003), forest soil (e.g., Mayer et al., 1995; Novák et al., 2001; Schoenau and Bettany, 1989; Tanikawa et al., 2018; Tanikawa et al., 2009; Turner et al., 2016), soil formed from carbonate bedrock (e.g., Mayer et al., 1995; Zhang et al., 2014), wetlands (e.g., Burton et al., 2011; Cao et al., 2018; Urban et al., 1989), and anthropogenically contaminated environments (e.g., Guo et al., 2016; Migaszewski et al., 2013).

Granitic rocks cover ~25% of the continental surface and play a crucial role in supplying nutrients to ecosystems at the earth's surface (Oliva et al., 2003). However, S deficiency occurs commonly in soils formed from granite because bedrock has a very low S content (Mayer et al., 1995). To the best of our knowledge, only one study reported the S dynamics in soils formed from granite in a cool and humid climate; however, its main focus was the source of SO_4^{2-} (Mayer et al., 1995). The authors of that study found that atmospheric deposition rather than mineral weathering was the main source of SO_4^{2-} in the soils, whereas a considerable portion of SO_4^{2-} in the subsoil leachates was derived from the mineralization of organic S. However, the sources and biogeochemical processes of S in the granitic profiles, particularly under contrasting climate, remain poorly understood.

The stable S isotope is a powerful tool in tracing the sources and biogeochemical processes of S in soils based on the isotopically different sources and the isotopic selectivity in biogeochemical processes (Novák et al., 2001; Xiao et al., 2015). The ^{32}S reacts preferentially during mineralization of organic S to aqueous SO_4^{2-} (Norman et al., 2002), whereas SO_4^{2-} uptake by vegetation and microorganisms slightly favors $^{34}SO_4^{2-}$ (Mayer et al., 1995). Moreover, the DSR leads to a significant depletion of sulfide in ^{34}S (Habicht and Canfield, 1997) even in oxidizing microhabitats in soils, albeit at a small reaction rate (Zhang et al., 2014). However, negligible isotope fractionation is observed during adsorption/desorption in aerated forest soils (Mayer et al., 1995).

In this study, we systematically investigated the S dynamics in soil profiles of four forest ecosystems of contrasting climate using the stable S isotope. A variety of soil chemical and mineralogical properties were measured, the results of which were used to interpret the S biogeochemical processes in the soils. Our main objectives were to investigate the biogeochemical processes controlling S dynamics in the soil profile and the effects of climatic and edaphic variables on S dynamics in soils. Overall, the present study provides an integration and synthesis of controls of climatic and edaphic variables on S dynamics in forest soils developed on granite.

2. Materials and methods

2.1. Study sites and soil sampling

Four soil profiles were developed on granite located in Oroqen Autonomous Banner, Inner Mongolia (NMG); Dunhua, Jilin (CBS); Longnan, Jiangxi (JLN); and Ledong, Hainan (HN) in China, respectively (Fig. 1a). These sites spread from northeast to southeast China, spanning 30° of latitude. The mean annual temperature (MAT) ranged from −0.4 °C to 25 °C and mean annual precipitation (MAP) from 480 mm to 1600 mm. Both the NMG and CBS profiles were located in a subhumid mid-temperate climate. The NMG site had a MAT of −0.4 °C and a MAP of 480 mm, whereas the CBS site had a MAT of 2.6 °C and a MAP of 598 mm. Two sites were covered with broadleaf forest. The JLN profile was located in a warm and humid subtropical climate with a MAT of 19 °C and a MAP of 1520 mm. The site was covered with evergreen broadleaf forest. The HN profile was located in the hot and humid tropical climate with a MAT of 25 °C and a MAP of 1600 mm. The site was dominated by evergreen broadleaf trees.

The four profiles, exposed in the study area as fresh road cuts, were sampled from top to bottom at fine depth intervals of 5 or 10 cm. The soil profiles were fresh and located in remote regions; thus, they were minimally affected by human activities. Because the profiles were also distant from agricultural areas, contamination from S fertilization was unlikely. Little disturbance from human earthworks and agricultural activities is further implied by uninterrupted changes in pH, soil organic carbon (SOC), and pedogenic Fe and Al concentrations with depth in all four profiles (data given below).

The slopes of the NMG, CBS, JLN, and HN profiles were 10°, 3°, 25°, and 3°, respectively, and the sampled profile thicknesses were 3 m, 2.5 m, 10 m, and 7 m, respectively. The soil horizons were designated according to the United States Soil Taxonomy (Soil Survey Staff, 2014). The A, B, and C horizons applied to the NMG, CBS, and JLN profiles; however, only the A and B horizons applied to the HN profile because the C horizons were too deep for sampling (Fig. 1b, Table S1). The soils of both NMG and CBS were classified as Ustic Dystrocryepts, JLN soil as a Typic Hapludult, and HN soil as a Typic Hapludox (Soil Survey Staff, 2014). Litter samples were collected at random from each site. Granite bedrock samples were collected from outcrops in close proximity to each soil profile.

2.2. Measurement of soil properties

The soil samples were air-dried and passed through 2-mm mesh sieves. The <2 mm samples were used for measurements of soil pH and particle size composition. Subsamples of the sieved soils and the granite rock samples were ball-milled to <200 mesh (75 μm) for measuring the concentrations of major elements, pedogenic Fe and Al minerals, and SOC, as well as for the total S concentration and stable S isotope analyses.

The soil pH was measured in 1:2.5 soil/CO_2-free deionized water suspensions using a glass electrode. The particle size composition was determined using a laser diffractometer (MasterSizer 2000, Malvern Panalytical, UK), following pretreatment with hydrogen peroxide to remove the organic component and chemical dispersion with sodium hexametaphosphate. According to the international size grades, the total fine earth (<2 mm) was fractionated into clay (0–2 μm), silt (2–20 μm) and sand (20–2000 μm).

The concentrations of major elements were determined by X-ray fluorescence (XRF) spectrometry (Axios, Malvern Panalytical, UK). Both the precision and accuracy were about 5%. The SOC concentrations were determined using an elemental analyzer (vario MACRO cube, Elementar, Germany) after decarbonation. The pedogenic Fe and Al were quantified by two-step extractions using an acidic (pH 3.2) ammonium oxalate solution (Fe_{ox}, Al_{ox}) (Schwertmann, 1964) followed by a citrate-dithionite solution (Fe_{di}, Al_{di}) (Holmgren, 1967). The total contents of pedogenic Fe ($Fe_{ox} + Fe_{di}$) and Al ($Al_{ox} + Al_{di}$) were calculated as the sum of oxalate and dithionate extractable Fe and Al, respectively.

The degree of chemical weathering was indicated by the Chemical Index of Alteration (CIA) (Nesbitt and Young, 1982) as

$$CIA = \frac{Al_2O_3}{Al_2O_3 + CaO^* + Na_2O + K_2O} \times 100, \quad (1)$$

where all constituent concentrations are expressed in mole/kg. In this equation, CaO* refers to the CaO incorporated only in silicates, not in apatite and carbonate, and is corrected using the method of McLennan (1993).

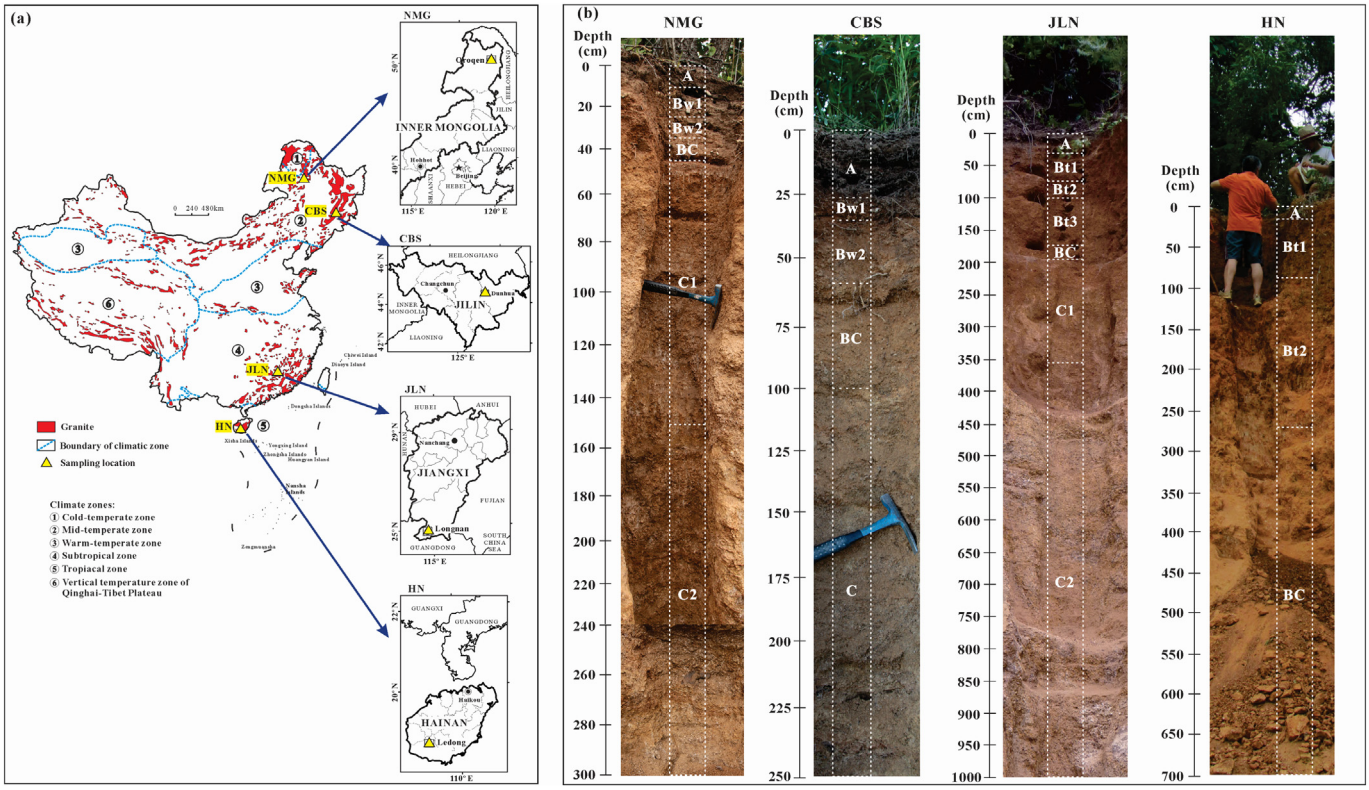

Fig. 1. (a) Location of the sampling sites in China, including Oroqen Autonomous Banner, Inner Mongolia (NMG); Dunhua, Jilin (CBS); Longnan, Jiangxi (JLN); Ledong, Hainan (HN). (b) Soil profiles showing horizon designations and depths.

2.3. Total S concentration and S isotope composition ($\delta^{34}S$) analyses

The soil, litter, and granite samples were mixed with Eschka's mixture at a ratio 1:4 and ignited at 800 °C. The produced SO_4^{2-} was dissolved in hot Milli-Q water and filtered. An aliquot from the filtrate was determined for the SO_4^{2-} concentration by routine ion chromatography (Dionex ICS-90, Thermo Scientific, Massachusetts, USA). The remaining filtrate was precipitated as $BaSO_4$ by adding a $BaCl_2$ solution. The resulting $BaSO_4$ was used to measure the $\delta^{34}S$ value of the SO_4^{2-}. The $\delta^{34}S$ value was expressed in per mil (‰) relative to the international Vienna Canyon Diablo Troilite standard using the equation

$$\delta^{34}S = (R_{sample}/R_{standard} - 1) \times 1000, \quad (2)$$

where $R = {}^{34}S/{}^{32}S$. All values incorporate an error of ±0.2‰.

2.4. Statistical analysis

The correlation analyses were conducted to evaluate the relationships between total S concentration and key soil chemical properties. Regression analyses were used to fit linear and allometric data by Origin 2018. Ordinary least squares linear fitting was used to analyze the relationships of total S concentration with silt and clay fractions, pH, and SOC content, and with the concentrations of $Fe_{ox} + Fe_{di}$ and $Al_{ox} + Al_{di}$ as well. Ordinary least squares allometric fitting was used to examine the relationships of total S concentration with the CIA value and sand fraction.

3. Results

3.1. Soil properties

The pH values of the NMG, CBS, JLN, and HN profiles were 4.8–6.9, 5.0–6.2, 4.6–6.7, and 3.4–5.8, respectively (Fig. 2a–d, Table S2). With increasing depth, the pH decreased to the minimum value in the subsurface (upper B horizons) and then increased downward for the NMG, CBS, and HN profiles. In the JLN profile, the pH monotonically increased with increasing depth. The SOC concentration was highest at the surface, at 111.8, 32.4, 39.9, and 41.0 mg/g for the NMG, CBS, JLN and HN profiles, respectively, and monotonically declined with depth, becoming very low or non-detectable below the B horizons (Fig. 2e–h, Table S2).

The pedogenic Fe ($Fe_{ox} + Fe_{di}$) concentrations were 5.0–12.4, 3.9–7.4, 8.8–23.8, and 7.9–26.9 mg/g (Fig. 2i–l, Table S2), whereas the pedogenic Al ($Al_{ox} + Al_{di}$) concentrations were 0.7–3.2, 1.0–2.3 mg/g, 2.2–6.4 mg/g, and 0.9–4.9 mg/g for the NMG, CBS, JLN, and HN profiles, respectively (Fig. 2m–p, Table S2). The pedogenic Fe and Al concentrations all reached maxima in the subsurface and decreased with depth across the four profiles.

The unweathered granite had CIA values of 51.2–58.3 (Fig. 2q–t, Table S2). The NMG and CBS profiles showed incipient to moderate weathering with CIA values of 60.8–70.5 and 56.7–62.0, respectively, whereas the JLN and HN profiles showed moderate to intensive weathering with the CIA values of 56.4–93.0 and 91.7–96.8, respectively (Fig. 2q–t).

Both the clay and silt fractions had higher proportions in the A and B horizons than those in the underlying horizons, whereas the sand fractions showed a reverse trend (Fig. 2u–w, Table S2). A significant threshold was observed at depths of 150, 100, and 400 cm for the NMG, CBS, and JLN profiles, respectively, with the highest sand content and lowest clay and silt contents. The A and B horizons in the JLN profile had higher proportions of clay and silt, at 9.6%–32.0% and 27.9%–52.7%, respectively, than those in the NMG and CBS horizons, with clay proportions of 5.1%–6.7% and 6.2%–8.7% and silt proportions of 32.4%–38.0% and 34.1%–45.5%, respectively. Considering that only the A and B horizons were sampled from the HN profile and composed mainly of fine particles, we did not measure its particle size composition.

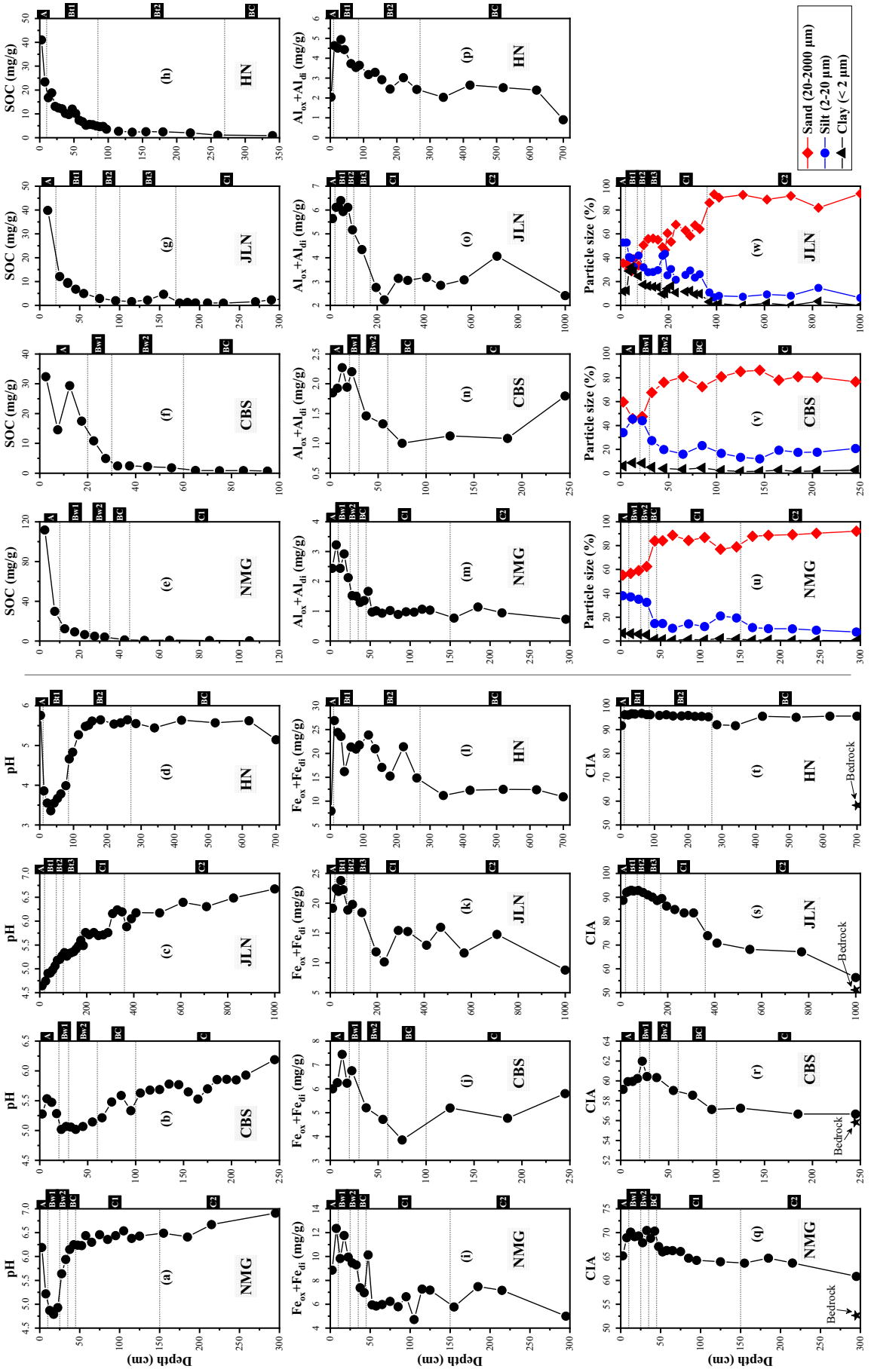

Fig. 2. pH (a, b, c, d), SOC (e, f, g, h), pedogenic Fe (Fe_{ox} + Fe_{di}, i, j, k, l), pedogenic Al (Al_{ox} + Al_{di}, m, n, o, p), CIA (q, r, s, t), and particle size composition (u, v, w) as a function of soil depth for the NMG, CBS, JLN, and HN profiles.

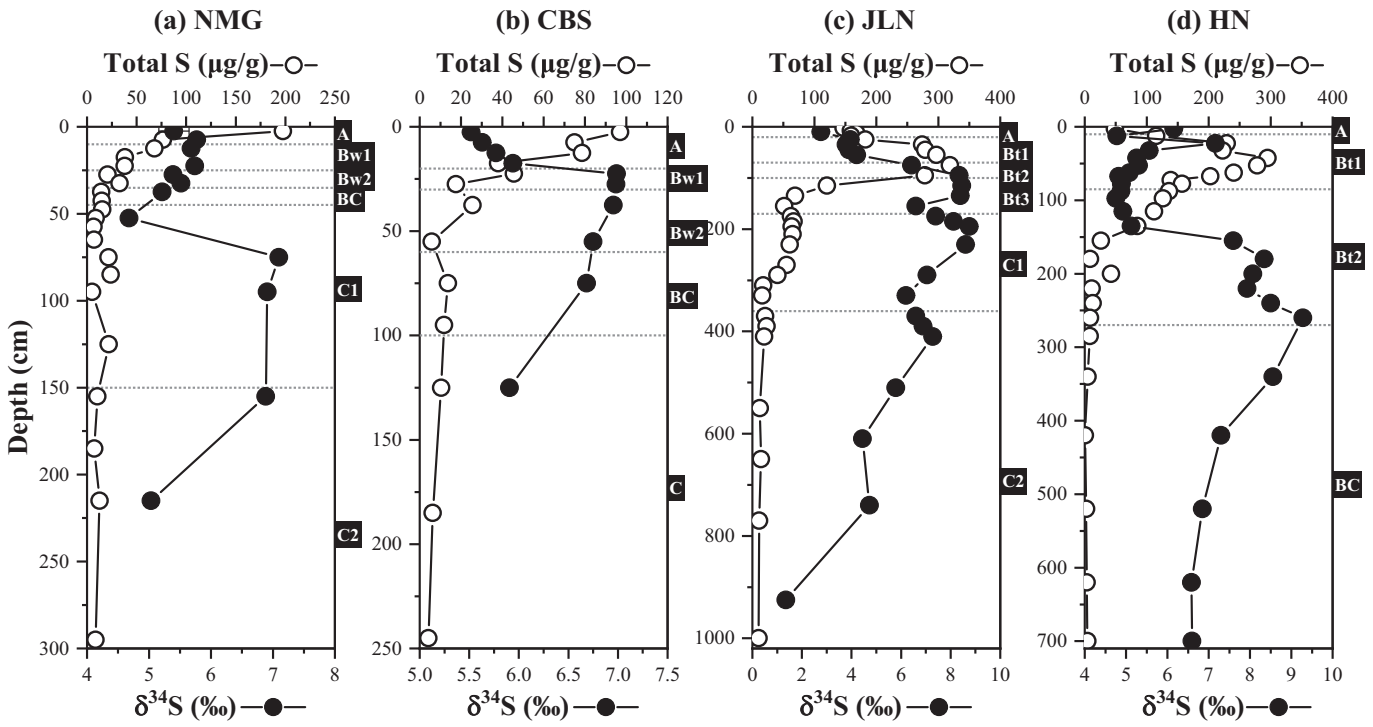

Fig. 3. Total S contents and $\delta^{34}S$ values of total S in NMG, CBS, JLN, and HN profiles.

3.2. Total S concentration and S isotope composition

The total S concentrations of the granite samples collected from the four sites ranged from 4.1 to 5.3 μg/g (Table S2); those of the litter samples ranged from 315 to 401 μg/g (Table S2). The total S concentrations of the NMG, CBS, JLN, and HN profiles were 5.2–197.5, 4.2–97.0, 9.9–318.9, and 0.2–295.0 μg/g, respectively (Fig. 3, Table S2). The total S concentrations monotonically declined with increasing depth for the NMG and CBS profiles (Fig. 3a, b). In the JLN and HN profiles, the total S concentrations increased from the surface to the subsurface and then sharply decreased toward the bottom of profiles (Fig. 3c, d).

The granite samples had an average $\delta^{34}S$ value of −1.62‰ (Table S2). The $\delta^{34}S$ values of the litter samples in the NMG, CBS, JLN, and HN profiles were 5.02‰, 4.35‰, 1.52‰, and 5.60‰, and those of the surface soils were 5.40‰, 5.52‰, 2.77‰, and 6.16‰, respectively. The ranges in $\delta^{34}S$ values for the four profiles were 4.68–7.09‰, 5.52–6.99‰, 1.35–8.76‰, and 4.75–9.28‰ for NMG, CBS, JLN, and HN, respectively (Fig. 3, Table S2). The $\delta^{34}S$ value showed a similar pattern in the CBS and JLN profiles such that it increased from the surface to the B horizon, remained constant at the high value in the B and upper C horizons, and finally gradually decreased toward the bottom (Fig. 3b, c). In the NMG and HN profiles, the $\delta^{34}S$ value generally followed the above pattern except for a remarkable decline in the B horizons.

3.3. Correlations between edaphic variables and soil S concentration

To understand the manner in which soil properties affect the total S distribution, we further explored the correlations between the total S concentration and the edaphic variables by compiling the data from all soil samples into one dataset regardless of climate and soil depth (Fig. 4). The total S concentration correlated positively with the CIA value ($R^2 = 0.66$, $p < 0.01$), silt content ($R^2 = 0.42$, $p < 0.01$), clay content ($R^2 = 0.7$, $p < 0.01$), $Fe_{ox} + Fe_{di}$ concentration ($R^2 = 0.47$, $p < 0.01$), and $Al_{ox} + Al_{di}$ concentration ($R^2 = 0.71$, $p < 0.01$), whereas the total S concentration correlated negatively with the sand content ($R^2 = 0.72$, $p < 0.01$) and pH ($R^2 = 0.46$, $p < 0.01$). For the NMG and CBS profiles, the total S concentration correlated significantly with the SOC content ($R^2 = 0.9$, $p < 0.01$). However, no significant correlation was present in the JLN and HN profiles ($R^2 = 0.08$, $p = 0.05$).

4. Discussion

4.1. Sulfur dynamics in soil profiles formed from granite

The $\delta^{34}S$ values in the surface soils, at 5.40‰, 5.52‰, 2.77‰, and 6.16‰, were similar to those in the litter, at 5.02‰, 4.35‰, 1.52‰, and 5.60‰ for the NMG, CBS, JLN, and HN profiles, respectively (Table S2). This suggests that the soil S is derived mainly from the overlying litter. Although we did not monitor the S concentration and isotope in the rainwater, atmospheric S can be mainly reflected in litter S through the assimilatory uptake of SO_4^{2-} by plants given that S in most parent materials of soils is low (Bern and Townsend, 2008), and this process has no significant S isotope fractionation (Krouse, 1991; Novák et al., 2001). Consistent with that reported in previous studies on ecosystems with S deficiency (e.g., Bern et al., 2015; Bern and Townsend, 2008; Turner et al., 2016), soil S is dominantly supplied as SO_4^{2-} in atmospheric deposition that is assimilated and temporarily stored in its high biomass before entering the soils as litter. Furthermore, the slightly higher $\delta^{34}S$ values in the surface soils than those in the litter indicate that S in surface soil is derived likely from decomposing litter and that the S is further enriched in recalcitrant organic matter (Norman et al., 2002). In addition, geogenic S from granite bedrock is also a possible S source for the soil profiles. Because granite has a very low S concentration of ~5 μg/g and negative $\delta^{34}S$ value of −1.62‰, geogenic S is unlikely to be the major source of S for the upper soil horizons. However, the deep soils (i.e., saprolite) have a low S concentration that is likely to be affected by geogenic input.

Given that litter inputs become weaker with increasing depth, the total S concentration is expected to decrease with increasing depth (Fig. 3). As expected, the NMG and CBS profiles show a monotonically decreasing total S concentration with depth. However, the JLN and HN profiles have the highest S concentration in the subsurface. This is because the warmer/wetter climate accelerates the mineralization of

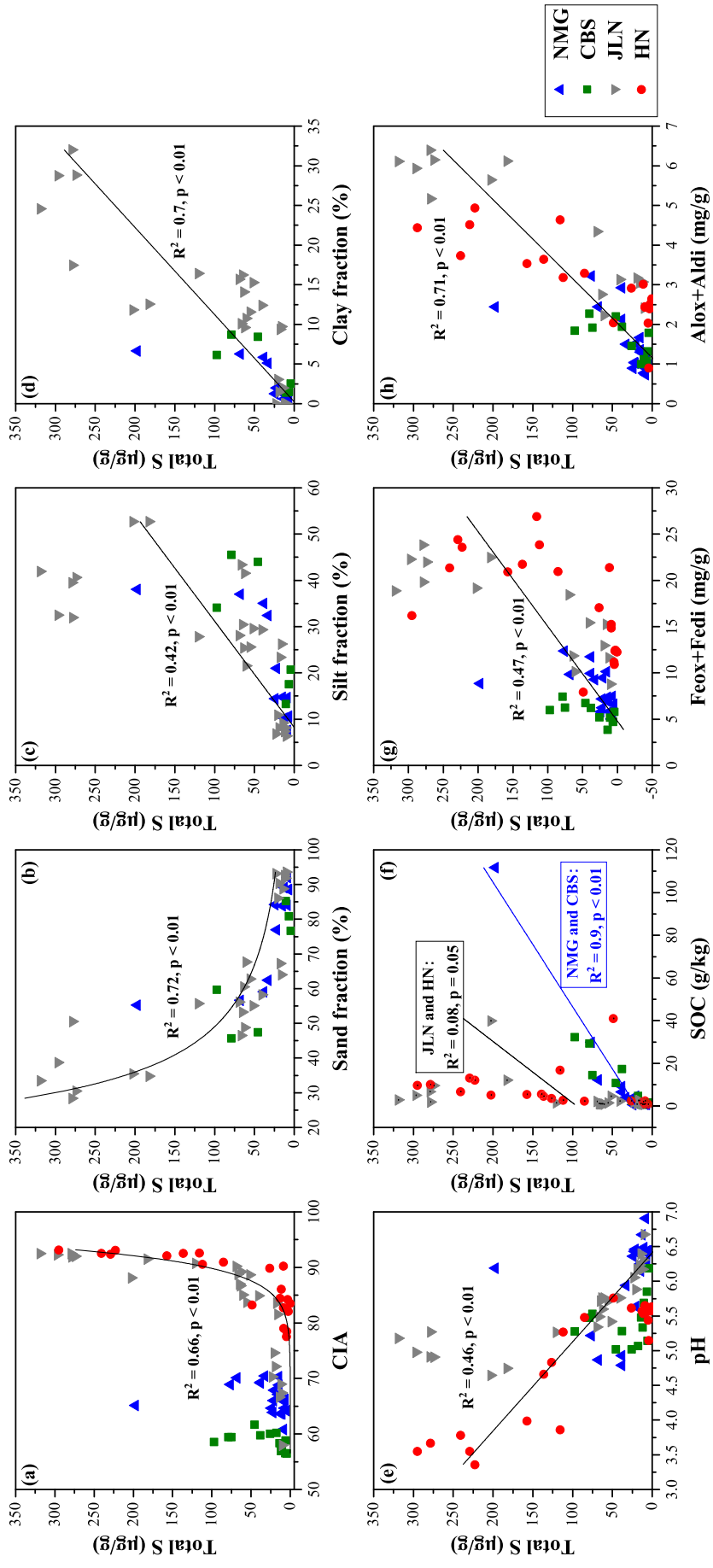

Fig. 4. Correlations between edaphic variables and total S concentration for the NMG, CBS, JLN and HN profiles regardless of soil depth and climate conditions. The correlation analyses in (f) were performed on two separate groups, with NMG and CBS as one group and JLN and HN as the second group; other trendlines were obtained from all the data. Ordinary least squares linear fitting was used in (c–h) and ordinary least squares allometric fitting was used in (a, b).

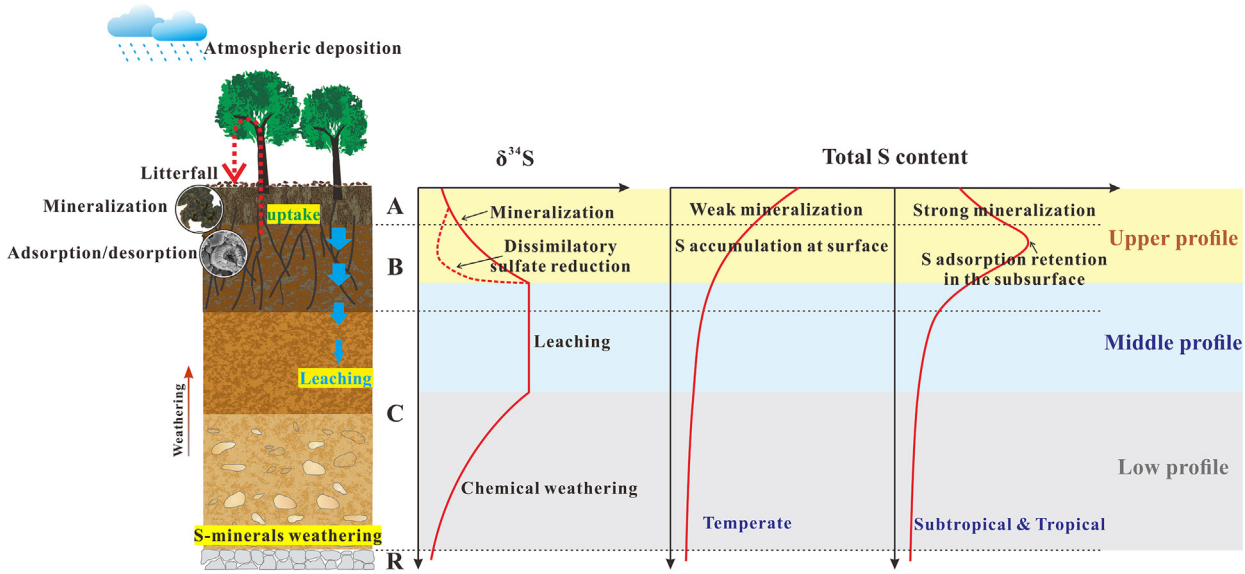

Fig. 5. Dominant biogeochemical processes pertinent to S at different depths in the forest soil profiles developed on granite and the schematic illustrations of the vertical distribution patterns of the total S concentration and $\delta^{34}S$ value.

organic S, and the released SO_4^{2-} esters and inorganic SO_4^{2-} are subsequently adsorbed onto pedogenic minerals in the subsurface. Therefore, SO_4^{2-} adsorption is an important S retention process for the subtropical and tropical climate because of the low pH and high pedogenic Fe/Al concentration in the subsurface (Fig. 2). In contrast, the colder/drier climate with weak mineralization and adsorption results in high organic S retention at the surface.

The $\delta^{34}S$ values generally follow a similar vertical distribution in the four soil profiles, although climate conditions and other soil formation factors affect the magnitude of fractionation. This similarity develops because all the profiles are shaped by the same set of pedogenic processes. Based on the results, we propose a conceptual model to describe the S dynamics in the soil profiles (Fig. 5). The conceptual model is summarized as (i) a downward increase in $\delta^{34}S$ values in the upper profiles due to continuous mineralization of organic S with an occasional decrease in $\delta^{34}S$ values in the subsurface due to DSR, (ii) constantly high $\delta^{34}S$ values in the middle profiles due to the low water permeability, and (iii) a downward decrease in $\delta^{34}S$ values in the low profiles due to the increased contribution of bedrock with depth. In the following, we discuss in details the biogeochemical processes of S at different depths.

For the upper profiles, the $\delta^{34}S$ values increase with increasing depth. The plant-derived C-bond S is first converted into SO_4^{2-} esters followed by their hydrolysis to inorganic SO_4^{2-}. The mineralization of organic S preferentially releases ^{32}S. Subsequent leaching leads to a loss of ^{32}S released from the organic S pool (Norman et al., 2002). Therefore, the continuous organic S mineralization and subsequent loss through leaching can explain the gradual decrease in total S concentration and increase in the $\delta^{34}S$ values with depth in the upper profiles. However, the total S concentration is highest in the subsurface of the JLN and HN profiles due to the strong sorption of pedogenic minerals, as discussed above, but the $\delta^{34}S$ values increase with depth. This is consistent with the fact that adsorption/desorption does not fractionate S isotopes due to rapid equilibration between adsorbed and solution SO_4^{2-} (Mayer et al., 1995). In addition, a decline in $\delta^{34}S$ values in the B horizons is observed in the NMG and HN profiles, which is most likely caused by DSR. The released SO_4^{2-} from mineralization of organic S is transported downward to the B horizons and then can undergo DSR conducted by anaerobic sulfate-reducing microorganisms. The DRS product is significantly depleted in ^{34}S compared with the precursory SO_4^{2-} (Krouse, 1991; Zhang et al., 2014), which can result in the low $\delta^{34}S$ values of total S in the B horizons of the NMG and HN profiles.

The low S concentrations and high $\delta^{34}S$ values are observed in the middle profiles. The organic and secondary SO_4^{2-} from mineralization of organic S are leached until reaching the soil-saprolite interface, where the permeability decreases sharply. This interface can be indicated by the particle-size distribution: a significant threshold of particle size with the highest sand content and lowest clay and silt contents is observed at depths of 150, 100, and 400 for the NMG, CBS, and JLN profiles, respectively (Fig. 2u–w). These depths are consistent with the deepest depths in which the total S is enriched in ^{34}S (Fig. 3). Therefore, downward leaching causes the accumulation of heavier S products in the middle profiles due to the low water permeability, which manifests as the constantly high $\delta^{34}S$ values.

The low profiles are influenced little by biological activities and leaching. The weathering degree decreases with increasing depth in the low profiles of the NMG, CBS and JLN sites (Fig. 2q–t). The general trend of decreasing $\delta^{34}S$ values with increasing depth can be explained by a two-source mixing model, in which S from one source (granite bedrock) is constant in concentration and isotopic composition, and that from a second source (leachate) of relatively high $\delta^{34}S$-value varies vertically in concentration. The contribution of granite bedrock to S concentration of the low profiles increases with increasing depth; thus the $\delta^{34}S$ values approach the bedrock value.

4.2. Effects of climate on sulfur dynamics

Climate is an important factor that can significantly affect the weathering intensity, soil chemistry and mineralogy, leaching, and biological activities (Jenny, 1941), which in turn affects the soil S dynamics. Our results show that the maximum $\delta^{34}S$ values in the middle profiles are 7.09‰, 6.99‰, 8.76‰ and 9.28‰ for the NMG, CBS, JLN, and HN profiles, respectively. For the upper profiles, the vertical variation in S isotopes is caused primarily by continuous mineralization of organic S and subsequent loss through leaching, as discussed above. The warmer/wetter climate at the JLN and HN sites shows more positive $\delta^{34}S$ values compared to the colder/drier climate at the NMG and CBS due to stronger intensity of organic S mineralization and leaching loss in the warmer/wetter climate.

Although bedrock weathering has no significant contribution to the soil S concentration due to the low S concentration in granite, the products of weathering (i.e., clay minerals and pedogenic Fe/Al minerals) strongly affect the S concentration in soils. The total S concentration positively correlates with the CIA value, soil clay content, and pedogenic

Fe/Al concentration (Fig. 4). Clay minerals and secondary Fe/Al minerals are known to strongly adsorb inorganic and organic SO_4^{2-} (Delmelle et al., 2003; Prietzel et al., 2007; Scott, 1976; Solomon et al., 2003; Tanikawa et al., 2018; Tanikawa et al., 2009). Thus, it is not surprising that warmer/wetter climate results in higher total S concentration in the subsurface, although the mineralization of organic P and loss through leaching are stronger. Our results emphasize the importance of SO_4^{2-}adsorption for S retention in the subtropical and tropical climate.

4.3. Controls of edaphic variables on soil S concentration

The total S concentration correlates well with the SOC for the NMG and CBS profiles (Fig. 4f), indicating that organic matter is the major source of S in soils formed from granite. However, this correlation is not observed in the JLN and HN profiles (Fig. 4f). This is because warmer/wetter climate accelerates the mineralization of organic matter, and the subsequently produced organic and secondary SO_4^{2-} are adsorbed onto the pedogenic minerals, as discussed above.

The total S concentration correlates well with the pH (Fig. 4e) likely because the adsorption/desorption of SO_4^{2-} depends on the soil pH (Prietzel et al., 2004). The high pH effectively prevents SO_4^{2-} adsorption; thus, SO_4^{2-} entering the soil can be considered as a mobile anion. Previous research has reported that SO_4^{2-} adsorption is negligible at pH > 5.5 (Prietzel et al., 2004), which is consistent with our results such that the total S concentration in soils is very low at pH > 6. Low pH can promote SO_4^{2-} adsorption to positively−charged surfaces of clay minerals and sesquioxides and thus the accumulation of SO_4^{2-} in the mineral soils (Nodvin et al., 1986; Prietzel et al., 2004).

The total S concentration correlates well with the concentrations of pedogenic Fe and Al minerals (Fig. 4g, h). This is consistent with the results of previous studies showing that pedogenic minerals stabilize organic S against microbial degradation in soils by, for example, inhibiting the hydrolysis of SO_4^{2-} esters (Prietzel et al., 2007; Solomon et al., 2003; Tanikawa et al., 2018; Tanikawa et al., 2009). Mechanisms that retain inorganic S, such as adsorption, precipitation, and occlusion by pedogenic minerals, can also contribute to S stabilization in soils (Delmelle et al., 2003; Scott, 1976). In particular, the total S concentration shows a stronger correlation with the pedogenic Al minerals than the Fe minerals, which implies that SO_4^{2-} adsorption is more dependent on pedogenic Al minerals (Scott, 1976). Among Al minerals, kaolinite and gibbsite, the most common secondary minerals derived from granite bedrock in the subtropical and tropical climate (Table S3), have the ability to adsorb both inorganic and organic SO_4^{2-} compounds (He et al., 1997; Rao and Sridharan, 1984).

5. Conclusions

We conducted a systematic investigation of S concentrations and S isotope compositions at different depths in four forest soil profiles developed on granite under contrasting climate conditions. We observed similar depth profiles of S isotope compositions from granite, litter, and soil horizons across different sites, implying similar S sources and consistent fractionation processes within forest ecosystems under contrasting climate conditions. Our isotope data suggest that incorporation of litter S is the main source of S in the upper soil horizons. Colder/drier climate with the weak mineralization and adsorption by pedogenic Fe/Al minerals, results in the high organic S retention at the surface. Although warmer/wetter climate increases the mineralization and leaching loss, SO_4^{2-} adsorption is an important S retention process in the subsurface due to the low pH and high pedogenic Fe/Al concentration therein. A conceptual model is proposed to describe the distribution patterns of the total S concentration and S isotope composition, and related processes, which provides a framework for understanding the manner in which pedogenesis redistributes and transforms S in the granitic profiles. We further found that the total S concentration correlated with the pedogenic Fe/Al minerals, suggesting the important role of secondary Fe/Al minerals in retaining S in soils. Future studies are warranted to confirm the relationships among the edaphic variables such as CIA, pH, SOC, and pedogenic Fe/Al minerals; the total S; and different S species using more diverse ecosystems.

CRediT authorship contribution statement

Zhuojun Zhang: Data curation, Formal analysis, Investigation, Methodology, Resources, Writing – original draft, Writing – review & editing. **Hairuo Mao:** Formal analysis, Methodology, Resources, Writing – original draft, Writing – review & editing. **Zhi-Qi Zhao:** Conceptualization, Formal analysis, Funding acquisition, Investigation, Project administration, Resources, Supervision, Validation, Writing – original draft, Writing – review & editing. **Lifeng Cui:** Investigation, Resources, Writing – review & editing. **Shilu Wang:** Supervision, Writing – review & editing. **Cong-Qiang Liu:** Conceptualization, Funding acquisition, Project administration, Supervision, Validation, Writing – review & editing.

Declaration of competing interest

The authors declare that they have no known competing financial interests or personal relationships that could have appeared to influence the work reported in this paper.

Acknowledgements

This work was funded by National Natural Science Foundation of China (Grant Nos. 41930863, 41661144042, and 41130536). The authors thank H. Ding, T. Liu, C. Tu, and B. Fan for collecting the soil samples used in this study.

Appendix A. Supplementary data

Supplementary data to this article can be found online at https://doi.org/10.1016/j.scitotenv.2021.149025.

References

Bern, C.R., Townsend, A.R., 2008. Accumulation of atmospheric sulfur in some Costa Rican soils. J. Geophys. Res. Biogeosci. 113, 13.
Bern, C.R., Chadwick, O.A., Kendall, C., Pribil, M.J., 2015. Steep spatial gradients of volcanic and marine sulfur in Hawaiian rainfall and ecosystems. Sci. Total Environ. 514, 250–260.
Burton, E.D., Bush, R.T., Johnston, S.G., Sullivan, L.A., Keene, A.F., 2011. Sulfur biogeochemical cycling and novel Fe–S mineralization pathways in a tidally re-flooded wetland. Geochim. Cosmochim. Acta 75, 3434–3451.
Cao, X., Wu, P., Zhou, S., Sun, J., Han, Z., 2018. Tracing the origin and geochemical processes of dissolved sulphate in a karst-dominated wetland catchment using stable isotope indicators. J. Hydrol. 562, 210–222.
Delmelle, P., Delfosse, T., Delvaux, B., 2003. Sulfate, chloride and fluoride retention in andosols exposed to volcanic acid emissions. Environ. Pollut. 126, 445–457.
Eriksen, J., 2009. Chapter 2 soil sulfur cycling in temperate agricultural systems. Advances in Agronomy. vol. 102. Academic Press, pp. 55–89.
Eriksen, J., Thorup-Kristensen, K., Askegaard, M., 2004. Plant availability of catch crop sulfur following spring incorporation. J. Plant Nutr. Soil Sci. 167, 609–615.
Freney, J.R., Williams, C.H., 1983. The sulfur cycle in soil. In: Ivanov, M.V., Freney, J.R. (Eds.), The Global Biogeochemical Sulphur Cycle. Scientific Committee on Problems of the Environment (SCOPE). vol. 19. Wiley, Chichester, pp. 129–201.
Guo, Q., Zhu, G., Strauss, H., Peters, M., Chen, T., Yang, J., et al., 2016. Tracing the sources of sulfur in Beijing soils with stable sulfur isotopes. J. Geochem. Explor. 161, 112–118.
Habicht, K.S., Canfield, D.E., 1997. Sulfur isotope fractionation during bacterial sulfate reduction in organic-rich sediments. Geochim. Cosmochim. Acta 61, 5351–5361.
He, L.M., Zelazny, L.W., Martens, D.C., Baligar, V.C., Ritchey, K.D., 1997. Ionic strength effects on sulfate and phosphate adsorption on γ-alumina and kaolinite: triple-layer model. Soil Sci. Soc. Am. J. 61, 784–793.
Hermes, A.L., Ebel, B.A., Murphy, S.F., Hinckley, E.-L.S., 2021. Fates and fingerprints of sulfur and carbon following wildfire in economically important croplands of California, U.S. Sci. Total Environ. 750, 142179.
Holmgren, G.G.S., 1967. A rapid citrate-dithionite extractable iron procedure. Soil Sci. Soc. Am. J. 31, 210–211.
Jenny, H., 1941. Factors of Soil Formation: A System of Quantitative Pedology. McGraw-Hill Book Company Inc, New York.

Krouse, H.R., 1991. Stable Isotopes: Natural and Anthropogenic Sulphur in the Environment. John Wiley and Sons, United Kingdom.
Marschner, H., 2011. Mineral Nutrition of Higher Plants. Academic press, San Diego.
Mayer, B., Feger, K.H., Giesemann, A., Jäger, H.-J., 1995. Interpretation of sulfur cycling in two catchments in the Black Forest (Germany) using stable sulfur and oxygen isotope data. Biogeochemistry 30, 31–58.
McLennan, S.M., 1993. Weathering and global denudation. J. Geol. 101, 295–303.
Migaszewski, Z.M., Gałuszka, A., Michalik, A., Dołęgowska, S., Migaszewski, A., Hałas, S., et al., 2013. The use of stable sulfur, oxygen and hydrogen isotope ratios as geochemical tracers of sulfates in the Podwiśniówka acid drainage area (south-central Poland). Aquat. Geochem. 19, 261–280.
Nesbitt, H.W., Young, G.M., 1982. Early Proterozoic climates and plate motions inferred from major element chemistry of lutites. Nature 299, 715–717.
Nodvin, S.C., Driscoll, C.T., Likens, G.E., 1986. The effect of pH on sulfate adsorption by a forest soil. Soil Sci. 142, 69–75.
Norman, A.L., Giesemann, A., Krouse, H.R., Jäger, H.J., 2002. Sulphur isotope fractionation during sulphur mineralization: results of an incubation–extraction experiment with a Black Forest soil. Soil Biol. Biochem. 34, 1425–1438.
Novák, M., Bottrell, S.H., Přechová, E., 2001. Sulfur isotope inventories of atmospheric deposition, spruce forest floor and living Sphagnum along a NW–SE transect across Europe. Biogeochemistry 53, 23–50.
Oliva, P., Viers, J., Dupre, B., 2003. Chemical weathering in granitic environments. Chem. Geol. 202, 225–256.
Prietzel, J., Mayer, B., Legge, A.H., 2004. Cumulative impact of 40 years of industrial sulfur emissions on a forest soil in west-central Alberta (Canada). Environ. Pollut. 132, 129–144.
Prietzel, J., Thieme, J., Salomé, M., Knicker, H., 2007. Sulfur K-edge XANES spectroscopy reveals differences in sulfur speciation of bulk soils, humic acid, fulvic acid, and particle size separates. Soil Biol. Biochem. 39, 877–890.
Rao, S.M., Sridharan, A., 1984. Mechanism of sulfate adsorption by kaolinite. Clay Clay Miner. 32, 414–418.
Schoenau, J.J., Bettany, J.R., 1989. 34S natural abundance variations in prairie and boreal forest soils. J. Soil Sci. 40, 397–413.
Schwertmann, U., 1964. Differentiation of soil iron oxides by extraction with ammonium oxalate-solution. Z. Pflanzenernähr. Düng. Bodenkd 105, 194–202.
Scott, N.M., 1976. Sulphate contents and sorption in scottish soils. J. Sci. Food Agric. 27, 367–372.
Soil Survey Staff, 2014. Keys to Soil Taxonomy. United States Department of Agriculture, Natural Resources Conservation Service, Washington, DC.
Solomon, D., Lehmann, J., Martínez, C.E., 2003. Sulfur K-edge XANES spectroscopy as a tool for understanding sulfur dynamics in soil organic matter. Soil Sci. Soc. Am. J. 67, 1721–1731.
Tanikawa, T., Takahashi, M., Imaya, A., Ishizuka, K., 2009. Highly accumulated sulfur constituents and their mineralogical relationships in Andisols from Central Japan. Geoderma 151, 42–49.
Tanikawa, T., Hashimoto, Y., Yamaguchi, N., Takahashi, M., Yoshinaga, S., 2018. Sulfur accumulation rates in volcanic soils of eastern Japan over the last millennium based on tephrochronology. Geoderma 315, 111–119.
Turner, B.L., Condron, L.M., France, C.A.M., Lehmann, J., Solomon, D., Peltzer, D.A., et al., 2016. Sulfur dynamics during long-term ecosystem development. Biogeochemistry 128, 281–305.
Urban, N.R., Eisenreich, S.J., Grigal, D.F., 1989. Sulfur cycling in a forested Sphagnum bog in northern Minnesota. Biogeochemistry 7, 81–109.
Wilhelm Scherer, H., 2009. Sulfur in soils. J. Plant Nutr. Soil Sci. 172, 326–335.
Xiao, H.-Y., Li, N., Liu, C.-Q., 2015. Source identification of sulfur in uncultivated surface soils from four Chinese provinces. Pedosphere 25, 140–149.
Zhang, W., Liu, C.-Q., Wang, Z.-L., Zhang, L.-L., Luo, X.-Q., 2014. Speciation and isotopic composition of sulfur in limestone soil and yellow soil in karst areas of southwest China: implications of different responses to acid deposition. J. Environ. Qual. 43, 809–819.